Effect of secondary electron emission on the plasma sheath

S. Langendorf and M. Walker

Citation: Physics of Plasmas (1994-present) **22**, 033515 (2015); doi: 10.1063/1.4914854
View online: http://dx.doi.org/10.1063/1.4914854
View Table of Contents: http://scitation.aip.org/content/aip/journal/pop/22/3?ver=pdfcov
Published by the AIP Publishing

Effect of secondary electron emission on the plasma sheath

S. Langendorf[1,2,a)] and M. Walker[1,2,b)]
[1]School of Aerospace Engineering, Georgia Institute of Technology, Atlanta, Georgia 30332, USA
[2]High-Power Electric Propulsion Laboratory, 625 Lambert St NW, Atlanta, Georgia 30318, USA

(Received 15 December 2014; accepted 28 February 2015; published online 30 March 2015)

In this experiment, plasma sheath potential profiles are measured over boron nitride walls in argon plasma and the effect of secondary electron emission is observed. Results are compared to a kinetic model. Plasmas are generated with a number density of 3×10^{12} m^{-3} at a pressure of 10^{-4} Torr-Ar, with a 1%–16% fraction of energetic primary electrons. The sheath potential profile at the surface of each sample is measured with emissive probes. The electron number densities and temperatures are measured in the bulk plasma with a planar Langmuir probe. The plasma is non-Maxwellian, with isotropic and directed energetic electron populations from 50 to 200 eV and hot and cold Maxwellian populations from 3.6 to 6.4 eV and 0.3 to 1.3 eV, respectively. Plasma Debye lengths range from 4 to 7 mm and the ion-neutral mean free path is 0.8 m. Sheath thicknesses range from 20 to 50 mm, with the smaller thickness occurring near the critical secondary electron emission yield of the wall material. Measured floating potentials are within 16% of model predictions. Measured sheath potential profiles agree with model predictions within 5 V ($\sim 1\ T_e$), and in four out of six cases deviate less than the measurement uncertainty of 1 V. © *2015 AIP Publishing LLC*. [http://dx.doi.org/10.1063/1.4914854]

I. INTRODUCTION

The description of plasma sheaths as space-charge layers that join plasmas to their boundaries is due to Langmuir and Child in the early 1900s and has since proven essential to the modern understanding of bounded plasmas.[1,2] Hobbs and Wesson extended the theory to include the possibility of electron emission from the wall,[3] which occurs in a number of applications including plasma thrusters, hollow cathode plasmas, emissive probes, and fusion plasmas. The Hobbs and Wesson theory predicts the existence of a space-charge limited regime for sheaths in which the electron emission from the wall becomes limited by the mutual repulsion of the emitted electrons. The results of recent simulations[4–6] and kinetic analyses[7,8] of sheaths over strongly emitting surfaces indicate that further sheath regimes exist beyond the limit of the Hobbs and Wesson theory. Several of these studies find that the sheath potential profile over an electrically isolated ("floating") emissive wall may flatten or reverse polarity.[4–8]

The new predictions of sheath regimes have driven renewed research activity concerning the interaction of electron emission and sheaths. Experiments using a thermionic emitting wall as an electron emission source were performed in the 1980s (Ref. 9) producing results qualitatively consistent with the Hobbs and Wesson theory. In 2012, Sheehan[2] and Li[10] investigated virtual cathode structures forming as a result of secondary electron emission (SEE) from conductive and dielectric-coated walls biased well below the plasma potential. These structures are outside the applicability of the Hobbs and Wesson theory due to its assumption of a floating wall. A first measurement of an inverse sheath structure over a floating wall using laser-induced fluorescence was presented in a 2012 conference,[11] but the authors are unaware of any further confirmation of the measurements. Thus, there is a need for additional investigation of the transition between low-SEE and high-SEE conditions of floating walls.

In this work, we measure sheath potential profiles over floating wall material samples and vary the primary electron energy of the plasma to manipulate the electron emission from the wall. The non-Maxwellian plasma that we investigate is not directly treated by the Hobbs and Wesson theory, so results are compared with a kinetic model generated using the formalism of Sheehan.[12] Sheaths are observed to decrease in potential to $\sim 1\ T_e$ in agreement with the predictions of theory for a near-critical SEE wall.[3–6] The structure of the paper is as follows: Section II describes the emitting sheath problem and a theoretical model, Section III details the experimental setup, and Sec. IV gives the experimental results and compares them with the model of Sec. II.

II. BACKGROUND

In the experimental portion of this work, we use a non-Maxwellian plasma with a significant fraction of energetic primary electrons to cause electron emission from the wall. Consequently, we cannot expect to compare results directly to the fluid theory of Hobbs and Wesson and must consider kinetic theories instead. The emitting sheath problem has been analyzed using kinetic theory by Schwager,[13] Sheehan,[10] and quite recently Rizopoulou.[14] For comparison with experimental work, Sheehan's model is convenient because it does not include the artificial "source sheath" that the other models employ to enable comparison with particle-in-cell (PIC) simulations. We cannot use Sheehan's model directly because it does not include a distribution function for the isotropic primary electrons that we find experimentally. These are electrons

a)Graduate Research Assistant. Author to whom correspondence should be addressed. Electronic mail: samuel.langendorf@gatech.edu.
b)Associate Professor. Electronic mail: mitchell.walker@ae.gatech.edu.

accelerated into the plasma device to a set energy, and confined through multiple bounces off of magnetic cusps such that their directionality is lost and their velocity distribution function (VDF) forms a spherical shell. We will refer to these scattered electrons as "isotropic" primary electrons to distinguish them from "beam" primary electrons, which have maintained their original directionality. In this section, we give the sheath model extension to include this isotropic primary electron population.

We assume that the sheath is 1-D, collisionless, free of ionization and recombination, free of magnetic fields, and composed solely of electrons and singly charged ions with mass ratio $\mu = m_i/m_e$. We consider the plasma electrons as a Maxwellian population at temperature T_{ep} and an isotropic monoenergetic population at energy E_i. The emitted electrons are considered to be half-Maxwellian at T_{ee}. Due to the low electron density/plasma frequency in the sheath (minimum wavelength for streaming instability[15] $\gg$ sheath thickness), we neglect the effect of instabilities between the distribution functions and couple them solely through the jointly determined electric field. The plasma ions enter the sheath with a number density n_0 and a directed energy E_0 or $\varepsilon_0 = E_0/T_{ep}$ towards the wall. The wall floats to the potential that balances positive and negative charge fluxes, $\phi_w = \phi_f$. The wall emission is set by the secondary electron yield γ, the average number of emitted electrons per incident electron.

This sheath has no sources and no sinks of particles except at the boundaries, so the system is an electrostatic Vlasov-Poisson system and the distribution functions do not change along the trajectories in phase space. Acceleration is due to the electric field only so the trajectory in (ϕ, v) space is known if the velocity at the boundary is known. Therefore, if the distribution function is known at the boundaries, the sheath can be fully solved. The electron distribution functions are given in Eqs. (1)–(3) and illustrated in Fig. 1. Equation (1) is the Maxwellian plasma electrons, repelled from the wall by the sheath potential. Equation (2) is the half-maxwellian emitted electrons from the wall, accelerated away from the wall by the sheath potential. Equation (3) is the isotropic primary electrons, which form a uniform distribution in 1D as can be shown by integrating the spherical-shell VDF over the non-normal dimensions. Electrons with sufficient velocity to reach the wall are depleted from the tails of the distribution functions, so the equations are piecewise in velocity according to Eqs. (4) and (5).

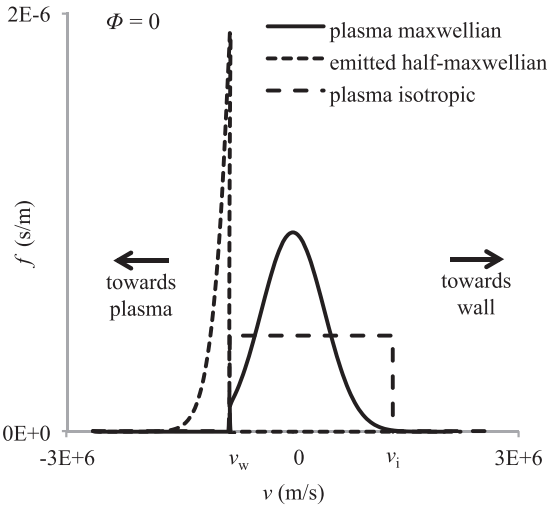

FIG. 1. Electron velocity distribution functions used in model, at $\phi = 0$ (sheath edge). Distributions are shown normalized such that at $\phi = 0$, their integral over all velocities is unity.

$$f_{ep}(v,\Phi) = \begin{cases} 0 & v \le v_w \\ \sqrt{\dfrac{m_e}{2\pi T_{ep}}}\exp\left(-\dfrac{m_e v^2}{2T_{ep}} - \Phi\right) & v > v_w, \end{cases} \quad (1)$$

$$f_{ee}(v,\Phi) = \begin{cases} \sqrt{\dfrac{2m_e}{\pi T_{ee}}}\exp\left(-\dfrac{m_e v^2}{2T_{ee}} + \theta(\Phi_w - \Phi)\right) & v \le v_w \\ 0 & v > v_w, \end{cases} \quad (2)$$

$$f_{ei}(v,\Phi) = \begin{cases} 0 & v \le v_w \\ \dfrac{1}{v_w(\Phi) + v_i(\Phi)} & v_w < v < v_i \\ 0 & v \ge v_i, \end{cases} \quad (3)$$

$$v_w(\Phi) = \sqrt{\frac{2T_{ep}}{m_e}(\Phi_w - \Phi)}, \quad (4)$$

$$v_i(\Phi) = \sqrt{\frac{2T_{ep}}{m_e}(\Phi_i - \Phi)}. \quad (5)$$

In Fig. 1 and Eqs. (2) and (4), $\Phi = \phi/T_{ep}$ and $\Phi_w = E_w/T_{ep}$, where E_w is the energy required to reach the wall. The emitted electron distribution f_{ep} is specified by the temperature ratio $\theta = T_{ep}/T_{ee}$. The isotropic electron distribution f_{ei} is specified by the energy $\Phi_i = E_i/T_{ep}$ and fraction $\alpha = n_{ei0}/(n_{ei0} + n_{ep0})$.

In this formulation, there are four unknown quantities: ε_0, Φ_w, and the normalization constants of the plasma and emitted electron distributions, which are the respective number densities. The number densities of the isotropic and Maxwellian plasma electrons are connected by the specification of α. We normalize the number densities of the plasma and emitted electron populations (n_{ep0} and n_{ee0}) at the boundary with respect to the ion number density n_0 as $N_{ep0} = n_{ep0}/n_0$ and $N_{ee0} = n_{ee0}/n_0$. To solve for the unknowns, we enforce the following constraints: quasineutrality at the sheath edge (6), the floating condition for balanced charge flux to the wall (7), the secondary emission yield relation between electron fluxes to and from the wall (8), and the marginal generalized Bohm criterion (9).

$$0 = 1 - N_{ep0} - N_{ee0} - \left(\frac{\alpha}{1-\alpha}\right)N_{ep0}, \quad (6)$$

$$0 = 1 - \frac{1}{\sqrt{\pi}}\frac{\exp(-\Phi_w)\sqrt{\dfrac{\mu}{\varepsilon}}}{2 - \operatorname{erfc}\left(\sqrt{\Phi_w}\right)}(N_{ep0}) + \frac{1}{\sqrt{\pi\theta}}\frac{\exp(-\Phi_w\theta)\sqrt{\dfrac{\mu}{\varepsilon}}}{\operatorname{erfc}\left(\sqrt{\Phi_w\theta}\right)}(N_{ee0}) - \frac{1}{2}\left(\frac{\alpha}{1-\alpha}\right)\left(\frac{\Phi_i - \Phi_w}{\sqrt{\Phi_i} + \sqrt{\Phi_w}}\right)(N_{ep0}), \quad (7)$$

$$0 = 0 - \frac{\gamma}{\sqrt{\pi}} \frac{\exp(-\Phi_w)\sqrt{\frac{\mu}{\varepsilon}}}{2 - \mathrm{erfc}\left(\sqrt{\Phi_w}\right)} (N_{ep0}) + \frac{1}{\sqrt{\pi\theta}} \frac{\exp(-\Phi_w\theta)\sqrt{\frac{\mu}{\varepsilon}}}{\mathrm{erfc}\left(\sqrt{\Phi_w\theta}\right)} (N_{ee0}) - \frac{\gamma}{2}\left(\frac{\alpha}{1-\alpha}\right)\left(\frac{\Phi_i - \Phi_w}{\sqrt{\Phi_i} + \sqrt{\Phi_w}}\right)(N_{ep0}), \quad (8)$$

$$0 = -\frac{1}{2\varepsilon} - \left(\frac{1}{\sqrt{\pi}} \frac{\exp(-\Phi_w)}{\sqrt{\Phi_w}\left(\mathrm{erfc}\left(\sqrt{\Phi_w}\right) - 2\right)} - 1\right)(N_{ep0}) - \left(\frac{1}{\sqrt{\pi}} \frac{\exp(-\Phi_w\theta)}{\sqrt{\Phi_w\theta}\,\mathrm{erfc}\left(\sqrt{\Phi_w\theta}\right)} - 1\right)(\theta)(N_{ee0}) + \frac{1}{2}\left(\frac{\alpha}{1-\alpha}\right)\left(\frac{1}{\sqrt{\Phi_i\Phi_w}}\right)(N_{ep0}). \quad (9)$$

In each of Eqs. (6)–(9), the four terms on the right side represent the contributions of the plasma ions, plasma Maxwellian electrons, emitted electrons, and plasma isotropic electrons, respectively. The equations are nonlinear but smooth, and thus can be solved numerically. Once the unknowns ε_0, Φ_w, N_{ep0}, and N_{ee0} are obtained, the sheath potential profile can be computed by integrating the electrostatic Poisson equation.

Fig. 2 below shows a result of this analysis, which is that the isotropic monoenergetic electron population can dictate the wall floating potential if it has sufficient energy and number density. As γ increases, the electric field at the wall decreases until it reaches zero at a critical $\gamma = \gamma_c$ (close to unity).

Fig. 2 shows the effect of the isotropic monoenergetic electron population on the wall floating potential. For a nonzero α, as Φ_i increases, Φ_w must increase to repel the energetic electrons and maintain balanced charge fluxes to the wall. At high Φ_i, the effect is similar to that of a directed beam of electrons as nearly all of the electrons have sufficient energy to impact the wall. The beam cannot push the floating potential higher than sits energy at $\Phi_i = 50$. The fraction of energetic electrons α affects the change in floating potential with γ: at low α, the floating potential decreases gradually as gamma increases, and at high α, the decrease occurs sharply.

If γ is known as a function of incident energy, it can be determined for a given plasma condition. Fig. 3 shows the solutions for Φ_w using data from the literature for γ of a BN wall.[16,17] The solutions become multi-valued in some regions for $\alpha > 0.035$, exhibiting a S-curve hysteresis. This is similar to some hysteresis curves shown for targets in fusion plasmas where the transition is caused by heat flux driving thermionic emission.[18,19] Here, it arises with a cold wall due to the high yield of the relatively scarce energetic isotropic electrons. The physical outcome is that there are multiple potentials the wall could assume and satisfy all of the constraints in the model (quasineutrality at sheath edge, charge flux conservation, SEE yield relation, and Bohm criterion). In practice, we expect that the solution branch that manifests physically will depend on the history of the plasma conditions in reaching that condition, for example, if Φ_i is started at a low value and steadily increased at $\alpha > 0.035$, the wall potential to follow the high potential branch until it enters the one-solution region at high Φ_i, manifesting in a step change in the wall potential.

III. EXPERIMENTAL SETUP

A. Multidipole plasma device

In this experiment, we use a multidipole plasma device. Multidipole devices have been used in many experiments since their invention in the early 1970s as a way to generate quiescent and spatially uniform plasmas.[20–23] The device used in these experiments consists of a cylindrical aluminum cage lined with permanent magnets. The magnets confine

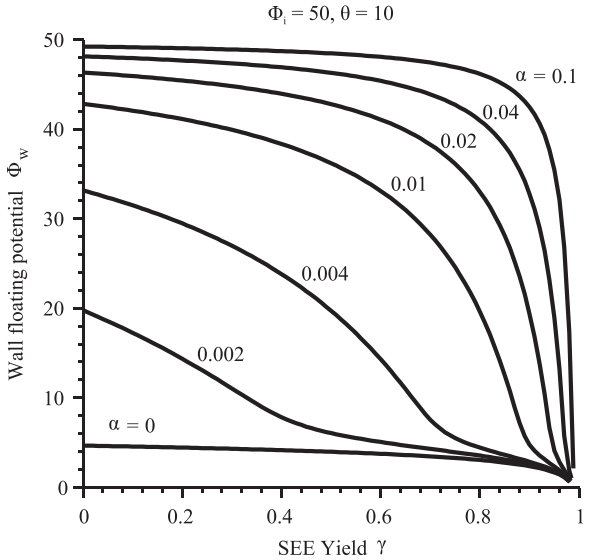

FIG. 2. Effect of electron emission yield γ and energetic isotropic electron fraction α on wall floating potential Φ_w for energy of isotropic electrons $\Phi_i = 50$ and a temperature ratio of plasma electrons to emitted electrons of $\theta = 10$.

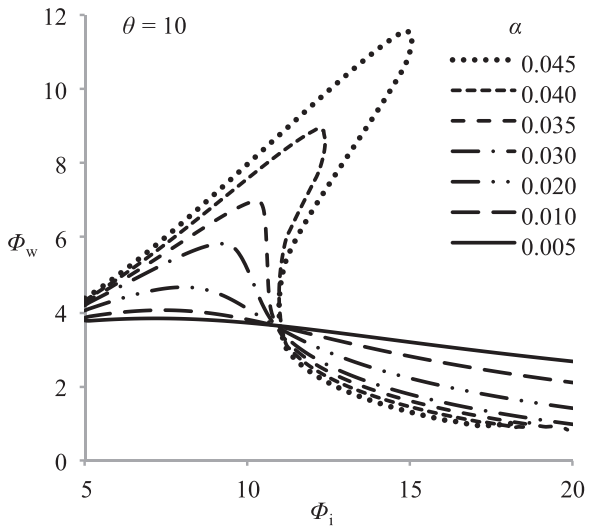

FIG. 3. Variation of normalized floating wall potential with increased energy of fast electron population. Solutions are multi-valued above a fraction of 3.5% fast electrons.

ionizing electrons generated by emissive filaments within the device. The cage is electrically grounded. The filaments are biased below ground and below the plasma potential to impart energy to the thermionically emitted electrons. Neutral molecules enter the device from the vacuum chamber. The mass flow input to the vacuum chamber is directed away from the plasma device to allow the gas to expand throughout the chamber and enter the plasma cell with a spatially uniform number density.

Fig. 4 shows a schematic of the multidipole plasma device used in this work. The interior length is 91.5 cm and the diameter is 61 cm. The construction is described in Ref. 24.

The plasma device is operated in the Georgia Institute of Technology Vacuum Test Facility-2, which is 9.2 m long, 4.9 m in diameter, and uses ten CVI TM1200i cryopumps to achieve a base pressure of 1.9×10^{-9} Torr.[25] In these experiments, the plasma device is positioned in the center of the chamber. Only two cryopumps are operated during this experiment in order to decrease pumping speed so that the desired experimental pressures can be obtained using a 500 sccm-N_2 range MKS 1179A01352CS1BV mass flow controller. This mass flow controller is used to flow 99.999% argon into the chamber and control the pressure. Pressure is measured with ±25% accuracy[26] using a Bayard-Alpert 571 ionization gauge connected to the vacuum chamber with a Varian XGS-600 gauge controller corrected for argon using a gas correction multiplier of 0.77. At the experimental pressure of 10^{-4} Torr-Ar, the ion-neutral mean free path is 0.8 m. Monitoring of vacuum chamber pressure did not show any pressure fluctuations within the ranged resolution of the ion gauge controller ($\pm 1 \times 10^{-5}$ Torr).

The five filaments are resistively heated in parallel using a TDK-Lambda 60V-25A DC power supply biased using a Keithley 2410 Sourcemeter. The discharge current is held constant at 10.0 mA in these experiments by manual adjustment of the filament heating current. The nominal value of the filament heating voltage and current is 7.34 V and 10.98 A, though it is adjusted throughout the experiment to account for drift in the discharge current. The discharge current exhibits drift on the order of 0.5 mA over 5 min, decreasing to 0.1 mA over 5 min after approximately 20 min of operation at a constant bias voltage. When drift in the discharge current occurs, it is held constant to 10.0 mA by manual hundredth-amp adjustments to the filament heating current.

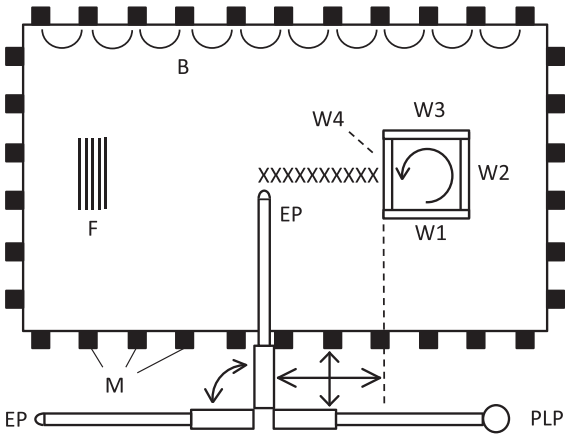

FIG. 4. Schematic of experimental layout. F = filaments, M = magnets, B = nominal magnetic field, PLP = planar Langmuir probe, EP = emissive probe, W = wall material sample, and X = nominal data measurement location. Emissive probe orientation rotated 90° in figure to show hairpin tip geometry. Figure not to scale.

B. Wall material samples

Two wall material samples of grade AX05 boron nitride are tested. The samples are 7.62 cm in diameter and 0.635 cm thick. One sample, the "smooth" wall, is polished using a Buehler Metaserv 250 grinder-polisher at 300 rpm. The "rough" wall sample is abraded with 120-grit SiC polishing paper. The resulting surface finishes are characterized using a LEXT OLS4000 profilometer. The average roughness of the rough sample (computed as the arithmetic mean of the absolute deviations in height from the mean height) is 10.4 μm averaged across five scans. The standard deviation of the average roughness between the five scans is 2.68 μm. The smooth surface had no roughness that could be observed within the profilometer resolution of 0.2 μm.

A cube-shaped stainless steel sample holder is positioned on centerline within the multidipole plasma device and supported on a rotation stage such that the different samples can be turned to the measurement position (W4 in Fig. 4). The two windows not holding the BN samples have quartz windows installed. The metal sample holder is electrically isolated from the plasma device to avoid giving the plasma electrons an alternative path to ground than the designed path across the cusp magnetic fields.

C. Diagnostics

The sheath potential profile is measured using an emissive probe as shown in Fig. 4. The Langmuir probe and an emissive probe are included on a rotation stage. The emissive probes are constructed of telescoping alumina tubing and a hairpin 0.127 mm diameter thoriated tungsten filament tip. The emissive probe is biased with a Keithley 2410 Sourcemeter. The probe is heated by a floating DC power supply until it has begun to glow in order to clean the probe tip, but only so hot that a small emission current (~50 μA) is observed. The emission current of the probe is determined by subtracting the cleaned cold probe characteristic from the hot emitting characteristic, so that the emission current is all that remains at biases below the plasma potential. The plasma potential is determined to be the voltage at which the inflection point of the probe characteristic occurs.[27] The resultant uncertainty is estimated at $T_e/5$, double that of the extrapolated method.[28] With both cold (~1 eV) and hot (~5 eV) electron populations present in the plasma, the accuracy is conservatively estimated at ±1 V. The emissive probe is positioned using a Parker 4062000XR linear motion table with a bi-directional repeatability of ±5 μm. The origin of the probe position is defined where the probe support touches the wall, which was determined to within ±125 μm.

Bulk plasma parameters are measured using a planar Langmuir probe positioned in the center of the plasma device. The Langmuir probe body is constructed of alumina tubing. The tip is made from 0.5 mm thick tungsten foil cut into a

circle of 7.70 mm diameter. Five linear stair sweeps from −200 to 0 V were collected and averaged with a dwell time of 20 ms at each voltage and a step interval of 0.2 V. The probe characteristics are corrected for singly charged argon ion- and electron-induced SEE using data for tungsten from Refs. 29 and 30 (degassed target), respectively. The probe is cleaned by ion bombardment at −500 V bias for a period of 15 min before data collection, after which time no noticeable change is observable in I-V characteristics. The probe is re-cleaned at −500 V for 30 s after the collection of each trace.

D. Langmuir probe processing

In order to achieve a low plasma density $\sim 10^{13}$ m^{-3} and measurable energetic electron populations, the plasma device is operated at a discharge current of 10 mA. The filament bias voltage is varied between −50 V and −200 V. The I-V characteristics obtained with the planar Langmuir probe do not show a prevalent "knee" and saturation of the collected current. Both the electron and ion collection regions show a linear relationship with voltage as typical of the orbital-motion-limited spherical probe. This indicates that the sheath thickness is significantly greater than the probe diffusion length of 3 mm, which is later supported by the emissive probe measurements of the sheaths over the wall material samples.

The Langmuir probe is interpreted in the following steps. An ion density and temperature are assumed to fit the ion collection region of the probe curve according to Eq. (10) (Ref. 31) and the fit ion current is subtracted out.

$$I_i = A_p n_i e \sqrt{\frac{k_B T_i}{2\pi M}} \left(1 - eV_p/kT_i\right). \tag{10}$$

In Eq. (10), I_i is the positive ion current collected by the Langmuir probe of area A_p at bias V_p with respect to the plasma potential, n_i and T_i are the ion number density and temperature, and M is the ion mass.

After the ion current has been fit as shown in Fig. 5 and subtracted out, the revealed energetic electron current (shown in Fig. 6) is observed to be composed of a directed-velocity "beam" component localized at the discharge voltage and an isotropic component. The beam component is fit by a linear fit spanning the voltage drop across the length of the discharge filament. A linear fit is used for the isotropic component following Hershkowitz *et al.*[32] Once the fits have been applied, the energetic electrons are subtracted out as well. The remaining electrons conform well to a bi-Maxwellian distribution as has been observed in multidipole argon plasmas at pressures near 10^{-4} Torr-Ar (Ref. 33) and fit accordingly. All fits are adjusted self-consistently to reduce error resulting in a constructed I-V curve that follows the collected data with relative error <1%.

IV. RESULTS AND DISCUSSION

A. Plasmas

The Langmuir probe is positioned 10 cm from the wall, where the primary electrons have already traversed most of the plasma device. Electron number densities are on the order of 3×10^{12} m^{-3}, detecting similar amounts of hot and cold Maxwellian electrons. Measured number densities and temperatures are plotted in Figs. 7 and 8 as a function of the bias voltage applied to the emitting filament. As shown in Fig. 8, the energetic electron populations gain energy directly through the increase of the filament bias. The changes in temperature of the hot and cold Maxwellian populations are on a lower order of magnitude, but show an increase when the filament is biased below −100 V. Fig. 7 shows that changing the filament bias does not result in a drastic change in the overall number densities or temperatures of the Maxwellian hot and cold electron populations as they vary between 3.6–6.4 eV and 0.3–1.3 eV. However, the number densities of the energetic electron populations decrease steadily. A portion of this decrease in number density is due to continuity, as the discharge current is held fixed. Additionally, this could be a result of increased energy exchange of the primary electrons with the plasma and contribute to the resurgence of the hot electron population, or it could be due to primary electrons increasingly escaping the magnetic cusps. The loss rate agrees with the literature that states that the loss half-width for energetic electrons through magnetic cusps scales directly with the gyroradius,[34] leading to the loss area scaling with electron energy.

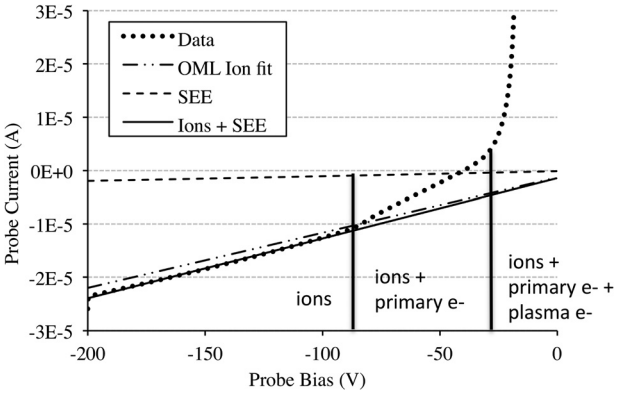

FIG. 5. Current traces obtained with planar Langmuir probe in the −90 V discharge voltage case, showing fit of ions and SEE. Regions where primary electrons and plasma electrons are collected are labeled.

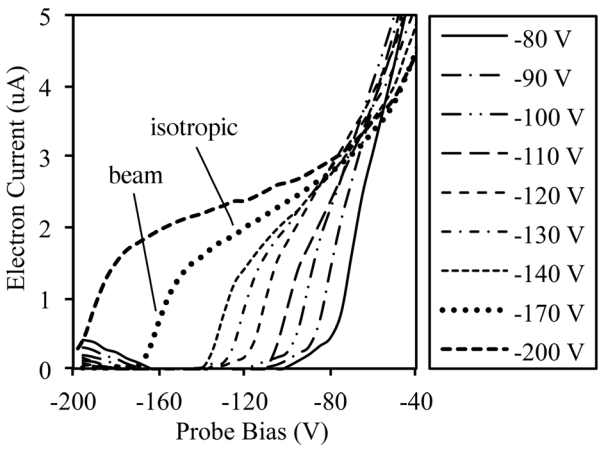

FIG. 6. Electron current traces obtained with planar Langmuir probe in the ion-collecting region (after subtraction of ion current). Collection of primary electrons is observed when the probe is biased above the discharge filament bias voltage.

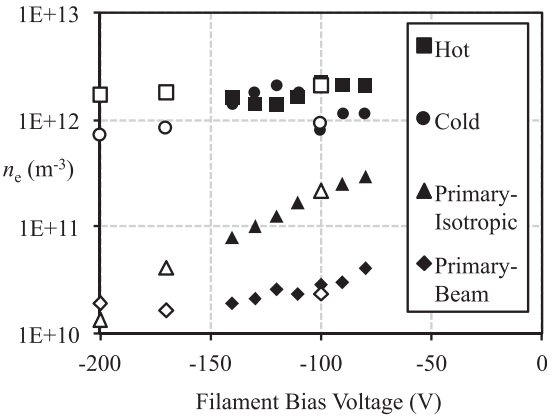

FIG. 7. Electron densities measured by planar Langmuir probe for varied bias of the discharge filament. Discharge current is 10 mA. Filled symbols are taken with smooth BN sample facing the discharge filament, open symbols with rough BN sample.

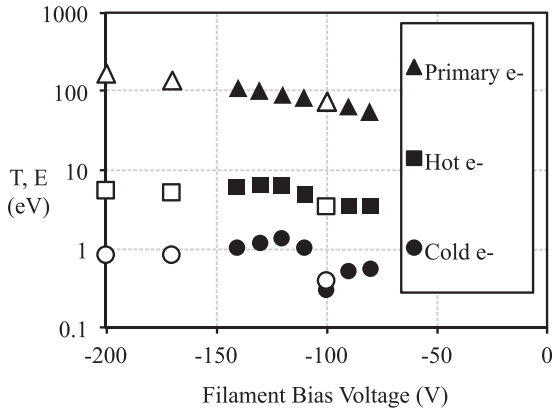

FIG. 8. Temperatures and energies measured by planar Langmuir probe for varied bias of the discharge filament. Primary electron energy is plotted, while temperature is plotted for the hot and cold electron population. Discharge current is 10 mA. Filled symbols are taken over smooth BN sample facing the discharge filament, open symbols over rough BN sample.

B. Sheaths

Fig. 9 shows the experimentally measured plasma potential (v_p) profiles over the rough and smooth BN wall material samples for a range of filament bias voltages (discharge voltage). The energy of the primary electrons follows the discharge voltage. The profiles are presented with respect to the bulk plasma potential (defined as the plasma potential measured 100 mm from the wall in each case).

Initially, as filament bias is driven more negative, the sheath potential is driven more negative in order to repel enough off-normal isotropic primary electrons to enforce zero net current to the electrically isolated wall. This agrees with the prior theoretical result that prevalent energetic electrons can drive the floating potential (cf. Fig. 2). However, once the filament bias passes a certain threshold, the SEE from the wall becomes too great to maintain a large sheath potential (the SEE yield of BN increases approximately linearly with energy in this range[35,36]). The transition between increasing and decreasing sheath potential is sharp, occurring fully within 20 V. This agrees with the theoretical s-curve prediction (cf. Fig. 3) for this level of primary electron fraction α (0.03–0.04). The sheath potential reaches the order of magnitude of the electron temperature of the hot electron population.

The sheath potential profiles over the rough and the smooth BN samples are the same within the measurement accuracy, except that the sheath over the smooth sample transitions to low sheath potential at a lower filament bias than the sheath over the rough sample. This is believed to be caused by the rough wall's geometrical obstruction and retention of secondary electrons that could otherwise escape, keeping it at a lower yield than the smooth wall for a given plasma condition. Very low yields have been observed in SEE yield measurements of walls with nanotubes aligned perpendicular to the wall, supporting the theory that a highly roughened geometry "catches" emitted electrons.[37]

Fig. 10 shows the experimentally measured Φ_w as a function of Φ_i compared to the predictions of the theoretical model. Since θ is unknown and γ is only known from the literature and not for the exact BN surface used, there is uncertainty in comparing the experimental results to theory. Each of the theoretical points lies on its own individual S-curve because each condition also has its own values of α and T_{ep}. There is also uncertainty in determining the experimental Φ_i due to the spread in energies of the primary electrons generated by the ~10 V voltage drop across the heated filaments (shown in Fig. 10 error bars). It can be seen in Fig. 9 that the results agree with the S-curve shape predicted by the model (cf. Fig. 3,) even for the arbitrarily chosen $\theta = 10$ and a linear fit for γ using data from references Refs. 13 and 14. Overall, the theory agrees with the measurements well outside the transition region of the S-curve, with a max relative error of 10.2%. In regions near the transition region, the

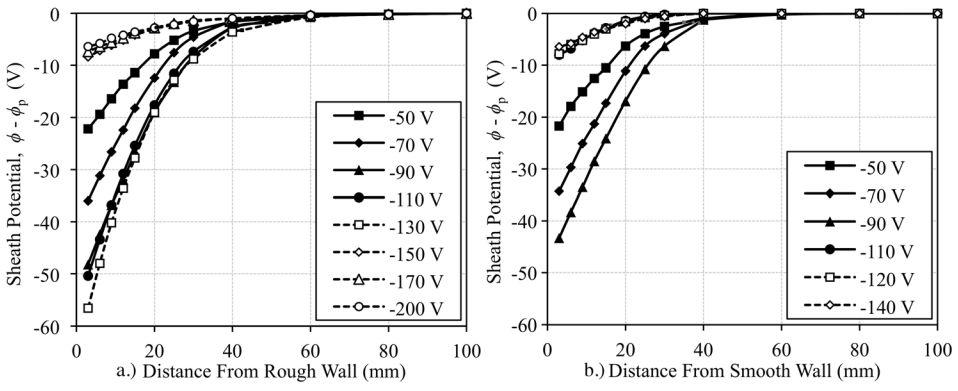

FIG. 9. Experimentally measured plasma potential profiles in the sheath over the (a) rough (Ra = 10.4 μm) and (b) smooth (Ra < 0.2 μm) BN wall material samples for different negative biases of the discharge filaments (labels = discharge voltage). Uncertainty in the potential is ±1 V, error bars not shown for clarity. Potentials are with respect to the sheath edge potential as measured at 100 mm from the wall.

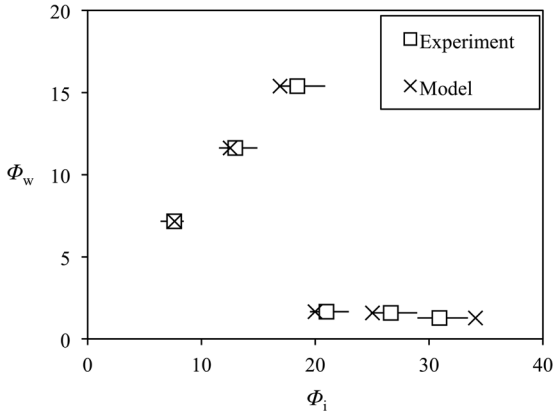

FIG. 10. Measured normalized wall potentials Φ_w vs. normalized energy of isotropic energetic electrons Φ_i.

comparison failed due to multiple solutions found by the theory.

Fig. 11 compares the experimentally measured sheaths to the computed sheaths from the kinetic model using measured plasma parameters from the Langmuir probe directly. We calculate the Debye length using a general form for multi-species plasma[38,39] shown in Eq. (11)

$$\frac{1}{\lambda_d{}^2} = \sum^{\alpha} \frac{1}{\lambda_{d,\alpha}{}^2} = \frac{1}{\lambda_{d,h}{}^2} + \frac{1}{\lambda_{d,c}{}^2}. \tag{11}$$

In Eq. (11), $\lambda_{d,c}$ and $\lambda_{d,h}$ are the Debye lengths calculated from the cold and hot electron populations, respectively. We found that including the scarce energetic populations in the summation in Eq. (11) made a negligible difference. Agreement is good overall for the cases shown but failed for the −110 V and −130 V cases; the theory found multiple solutions. For the −70 V, −150 V, −170 V, and −200 V cases, the model agrees with the data within the experimental error of ±1 V. In the −50 V case, the computed wall potential agrees well with the experiment but the sheath thickness does not. This is the only case in which there seems to be a large error in the Debye length measured from the Langmuir probe. If the Debye length is manipulated to be 50% greater than the value calculated from the measurements, the resulting profile agrees with the data within the measurement error. In the −90 V case, the Debye length is appropriate but the wall potential prediction is about 4 V too low resulting in a computed sheath offset 4 V from the experimental data. This could be a result of the experimental uncertainty in determining Φ_i; if Φ_i is manipulated to be 8% less than measured and the Debye length is decreased by 10%, the resulting profile agrees within the experimental error of 1 V.

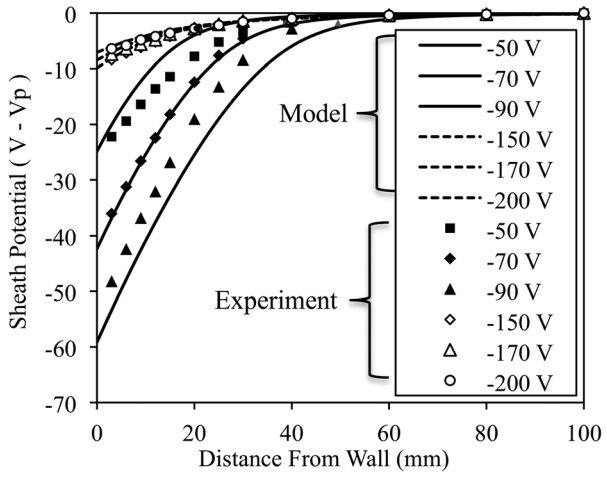

FIG. 11. Comparison of model-predicted sheath potential profiles with experimental data. Experimentally measured values are input for α, Φ_i, $T_e = T_{eh}$, and λ_D, θ is assumed = 10, and linear fit to γ for BN from Refs. 32 and 33 are used in the model of Sec. II to generate the theoretical profiles.

V. CONCLUSIONS

Overall, we find that measured sheaths agree well with the behavior predicted by kinetic theory in cases where the plasma is far from the transition region between high and low sheath potentials. In the case where the plasma is near to the transition condition, the direct theoretical prediction could not be reconciled with the data. This is perhaps unsurprising due to the experimental uncertainty and the steep gradients/multiple solutions predicted for the wall potential. A fruitful approach for future experiments to resolve this region would be to take measurements in order of increasing primary electron energy, then decreasing, in an effort to observe any hysteresis behavior of the sheath potential predicted by theory. In all sheaths measured, the calculated electron emission from the wall stayed below the critical value near unity, allowing the sheaths to be modeled by the theory presented. No sheaths were measured with lower sheath potential than predicted by the Hobbs and Wesson theory, although the kinetic model suggests that the potential can continue to decrease to a limiting value set by the ratio of emitted electron temperature to plasma electron temperature. It is yet to be determined what happens to the sheath when the electron yield exceeds the critical value and becomes greater than unity.

ACKNOWLEDGMENTS

This work was supported by the Air Force Office of Scientific Research through Grant No. FA9550-11-10160. The authors would like to thank Aaron Schinder and Natalie Schloeder for helpful discussion.

[1]C. D. Child, "Discharge from hot CaO," Phys. Rev. **32**(5), 492 (1911).
[2]I. Langmuir, "The effect of space charge and residual gases on thermionic currents in high vacuum," Phys. Rev. **2**(6), 450 (1913).
[3]G. D. Hobbs and J. A. Wesson, "Heat flow through a Langmuir sheath in the presence of electron emission," Plasma Phys. **9**, 85 (1967).
[4]M. D. Campanell, A. V. Khrabrov, and I. D. Kaganovich, "Absence of Debye sheaths due to secondary electron emission," Phys. Rev. Lett. **108**, 255001 (2012).
[5]D. Sydorenko, I. Kaganovich, Y. Raitses, and A. Smolyakov, "Breakdown of a space charge limited regime of a sheath in a weakly collisional plasma bounded by walls with secondary electron emission," Phys. Rev. Lett. **103**(14), 145004 (2009).
[6]M. D. Campanell, A. V. Khrabrov, and I. D. Kaganovich, "General cause of sheath instability identified for low collisionality plasmas in devices with secondary electron emission," Phys. Rev. Lett. **108**(23), 235001 (2012).

[7]J. P. Sheehan, "The effects of space-charge limited electron emission on the plasma sheath," Ph.D. dissertation (University of Wisconsin-Madison, 2012).
[8]M. D. Campanell, "Negative plasma potential relative to electron-emitting surfaces," Phys. Rev. E **88**(3), 033103 (2013).
[9]T. Intrator, M. H. Cho, E. Y. Wang, N. Hershkowitz, D. Diebold, and J. DeKock, "The virtual cathode as a transient double sheath," J. Appl. Phys. **64**(6), 2927–2933 (1988).
[10]W. Li, J. X. Ma, J. J. Li, Y. B. Zheng, and M. S. Tan, "Measurement of virtual cathode structures in a plasma sheath caused by secondary electrons," Phys. Plasmas **19**(3), 030704 (2012).
[11]N. Claire and F. Doveil, "Ion velocity distribution functions in the positive sheath of an insulated BNSiO2 surface in a plasma," in *39th EPS Conference and 16th International Congress on Plasma Physics* (2012), P1.174.
[12]J. P. Sheehan, I. D. Kaganovich, H. Wang, D. Sydorenko, Y. Raitses, and N. Hershkowitz, "Effects of emitted electron temperature on the plasma sheath," Phys. Plasmas **21**(6), 063502 (2014).
[13]L. A. Schwager and C. K. Birdsall, "Collector and source sheaths of a finite ion temperature plasma," Phys. Fluids B **2**(5), 1057–1068 (1990).
[14]N. Rizopoulou, A. P. L. Robinson, M. Coppins, and M. Bacharis, "Electron emission in a source-collector sheath system: A kinetic study," Phys. Plasmas **21**(10), 103507 (2014).
[15]S. N. Kathuria and G. L. Kalra, "Two-stream instability in a collisionless plasma," Astrophys. Space Sci. **24**(1), 133 (1973).
[16]V. Viel-Inguimbert, "Secondary electron emission of ceramics used in the channel of SPT," in 28th International Electric Propulsion Conference, Toulouse, France, 2003, IEPC-2003-258.
[17]P. H. Dawson, "Secondary electron emission yields of some ceramics," J. Appl. Phys. **37**, 3644 (1966).
[18]S. Takamura, M. Y. Ye, T. Kuwabara, and N. Ohno, "Heat flows through plasma sheaths," Phys. Plasmas **5**(5), 2151–2158 (1998).
[19]M. Y. Ye, S. Masuzaki, K. Shiraishi, S. Takamura, and N. Ohno, "Nonlinear interactions between high heat flux plasma and electron-emissive hot material surface," Phys. Plasmas **3**(1), 281–292 (1996).
[20]L. Oksuz and N. Hershkowitz, "Plasma, presheath, collisional sheath and collisionless sheath potential profiles in weakly ionized, weakly collisional plasma," Plasma Sources Sci. Technol. **14**(1), 201 (2005).
[21]D. Lee, G. Severn, L. Oksuz, and N. Hershkowitz, "Laser-induced fluorescence measurements of argon ion velocities near the sheath boundary of an argon–xenon plasma," J. Phys. D: Appl. Phys. **39**(24), 5230 (2006).
[22]R. Limpaecher and K. R. Mackenzie, "Magnetic multipole containment of large uniform collisionless quiescent plasmas," Rev. Sci. Instrum. **44**(6), 726–731 (1973).
[23]A. Lang and N. Hershkowitz, "Multidipole plasma density," J. Appl. Phys. **49**, 4707 (1978).
[24]S. J. Langendorf, M. L. R. Walker, L. Rose, M. Keidar, and L. Brieda, "Wall material effects on sheath potential profile," in *Proceedings of the 49th AIAA/ASME/SAE/ASEE Joint Propulsion Conference, San Jose, CA, July 14–17* (2013), AIAA 2013-4128.
[25]A. W. Kieckhafer and M. L. R. Walker, "Recirculating liquid nitrogen system for operation of cryogenic pumps," in Proceedings of the 32nd International Electric Propulsion Conference, Hamburg, Germany, September 2011.
[26]See http://www.thinksrs.com/downloads/PDFs/ApplicationNotes/IG1BAGapp.pdf for Stanford Research Systems, Appl. Note "Bayard-Alpert ionization gauges," p. 38 [cited 1 July 2013].
[27]V. A. Godyak and R. B. Piejak, "Probe measurements of the space potential in a radio-frequency discharge," J. Appl. Phys. **68**, 3157–3162 (1990).
[28]J. P. Sheehan and N. Hershkowitz, "Emissive probes," Plasma Sources Sci. Technol. **20**(6), 063001 (2011).
[29]H. D. Hagstrum, "Theory of Auger ejection of electrons from metals by ions," Phys. Rev. **96**(2), 336 (1954).
[30]R. M. Chaudhri, "Secondary electron emission from tungsten," in *Proceedings of the National Institute of Sciences of India* (National Institute of Sciences of India, 1941), Vol. 7, p. 197.
[31]J. E. Allen, "Probe theory-the orbital motion approach," Phys. Scr. **45**(5), 497 (1992).
[32]N. Hershkowitz, J. R. DeKock, P. Coakley, and S. L. Cartier, "Surface trapping of primary electrons by multidipole magnetic fields," Rev. Sci. Instrum. **51**(1), 64–69 (1980).
[33]E. Stamate, K. Inagaki, K. Ohe, and G. Popa, "On energetic electrons in a multipolar magnetically confined Ar plasma," J. Phys. D: Appl. Phys. **32**(6), 671 (1999).
[34]K. N. Leung, N. Hershkowitz, and K. R. MacKenzie, "Plasma confinement by localized cusps," Phys. Fluids **19**(7), 1045–1053 (1976).
[35]V. Viel-Inguimbert, "Secondary electron emission of ceramics used in the channel of SPT," in 28th International Electric Propulsion Conference, Toulouse, France, March 2003, IEPC-2003-258.
[36]J. P. Bugeat and C. Koppel, "Development of a second generation of SPT," in 24th International Electric Propulsion Conference, Moscow, Russia, 1995, IEPC-95-035.
[37]Y. Raitses, I. D. Kaganovich, and A. V. Sumant, "Electron emission from nano-and micro-engineered materials relevant to electric propulsion," in Proceedings of the 33rd International Electric Propulsion Conference, Washington DC, USA, 2013.
[38]J. D. Callen, *Fundamentals of Plasma Physics*, Chap. 1; see http://homepages.cae.wisc.edu/~callen for online book.
[39]See http://www.encyclopediaofmath.org/index.php?title=Debye_length&oldid=33810 for Debye length. Encyclopedia of Mathematics.